Changes in resource partitioning between and within organs support growth adjustment to neighbor proximity in *Brassicaceae* seedlings

Mieke de Wit[a,1,2], Gavin M. George[b,1], Yetkin Çaka Ince[a], Barbara Dankwa-Egli[b,3], Micha Hersch[c,d], Samuel C. Zeeman[b], and Christian Fankhauser[a,4]

[a]Center for Integrative Genomics, Faculty of Biology and Medicine, University of Lausanne, CH-1015 Lausanne, Switzerland; [b]Plant Biochemistry, Institute of Molecular Plant Biology, ETH Zurich, 8092 Zurich, Switzerland; [c]Department of Computational Biology, University of Lausanne, CH-1015 Lausanne, Switzerland; and [d]Swiss Institute of Bioinformatics, CH-1015 Lausanne, Switzerland

Edited by Winslow R. Briggs, Carnegie Institution for Science, Stanford, CA, and approved September 4, 2018 (received for review April 9, 2018)

In shade-intolerant plants, the perception of proximate neighbors rapidly induces architectural changes resulting in elongated stems and reduced leaf size. Sensing and signaling steps triggering this modified growth program have been identified. However, the underlying changes in resource allocation that fuel stem growth remain poorly understood. Through $^{14}CO_2$ pulse labeling of *Brassica rapa* seedlings, we show that perception of the neighbor detection signal, low ratio of red to far-red light (R:FR), leads to increased carbon allocation from the major site of photosynthesis (cotyledons) to the elongating hypocotyl. While carbon fixation and metabolite levels remain similar in low R:FR, partitioning to all downstream carbon pools within the hypocotyl is increased. Genetic analyses using *Arabidopsis thaliana* mutants indicate that low-R:FR–induced hypocotyl elongation requires sucrose transport from the cotyledons and is regulated by a PIF7-dependent metabolic response. Moreover, our data suggest that starch metabolism in the hypocotyl has a growth-regulatory function. The results reveal a key mechanism by which metabolic adjustments can support rapid growth adaptation to a changing environment.

neighbor proximity detection | resource partitioning | starch | PIF7 | phytochrome B

To withstand environmental challenges, plants have a remarkably plastic phenotype, allowing them to optimize their architecture for the prevailing circumstances. Shade-intolerant plants compete for light with their neighbors, typically by accelerating growth of stem-like structures to bring their leaves toward the light in the so-called shade avoidance response (1). This enhanced stem elongation is reflected in increased biomass accumulation in stems, while growth of leaves, roots, and seeds is often reduced (2–6).

The presence of neighboring plants is perceived by the phytochrome (phy) photoreceptors, which detect a drop in the ratio of red to far-red light (R:FR) due to increased levels of FR reflected off green plant tissue (7). Given that FR light does not contribute to photosynthetically active radiation (PAR), a low-R:FR environment can be established through FR supplementation without affecting PAR. Similarly, a shade avoidance response can be induced by end-of-day exposure to FR (EOD-FR), which inactivates phys at the beginning of the night. Low R:FR inactivates phys, relieving repression of the PHYTOCHROME INTERACTING FACTORs (PIFs) 4, 5, and 7 (8, 9). The PIFs subsequently activate an array of targets, including genes related to processes of auxin biosynthesis, transport, signaling, and cell wall biogenesis and modification (9, 10). While there appears to be a core set of shade avoidance genes (11), expression patterns become increasingly organ specific over time in *Arabidopsis* seedlings, which likely reflects the different growth responses of hypocotyl (embryonic stem) and cotyledons (embryonic leaves) (12).

Surprisingly little is known about metabolic changes involved in the shade avoidance response. Considering the major investment in stem growth, there must be considerable changes in resource partitioning while under the threat of light limitation. Photosynthates are transported through the phloem in the form of sucrose from high production sites (source) to organs in carbon deficit (sink) (13, 14). This was addressed in experiments in which radiolabeled carbon in the form of ^{14}C-urea was brushed onto the first pair of leaves of stem-forming plants. Such a treatment leads to release of $^{14}CO_2$, through urea uptake and endogenous enzymatic hydrolysis, which can be taken up by the plant during photosynthesis. More ^{14}C was recovered in internodes from sunflower plants (*Helianthus annuus*) that had been treated with 3 d of low R:FR compared with internodes from plants in high R:FR (15). In a similar experiment using ^{14}C urea, 24 h of low-R:FR treatment led to enhanced allocation of ^{14}C to the first internode of *Sinapis alba*, whereas a lower proportion of ^{14}C remained in the leaves of the plant (16). As the total amount

Significance

In dense communities, plants compete for light and sense potentially threatening neighbors prior to actual shading. In response to neighbor proximity cues, shade-intolerant plants selectively elongate stem-like structures, thereby enhancing access to unfiltered sunlight. Although key steps in plant proximity sensing and signaling have been identified, we know little about the metabolic adaptations underlying enhanced stem growth. Here, we show that, following the detection of neighbor proximity cues, seedlings allocate more carbon fixed in the cotyledons to the faster elongating hypocotyl. Moreover, we show that sucrose transport and a transcription factor responding to light and metabolic cues control hypocotyl elongation. Collectively, our work provides important insights into the metabolic changes underlying organ-specific growth adaptations to an environmental stress signal.

Author contributions: M.d.W., G.M.G., M.H., S.C.Z., and C.F. designed research; M.d.W., G.M.G., Y.Ç.I., B.D.-E., and M.H. performed research; M.d.W., G.M.G., Y.Ç.I., B.D.-E., M.H., S.C.Z., and C.F. analyzed data; and M.d.W., G.M.G., and C.F. wrote the paper.

The authors declare no conflict of interest.

This article is a PNAS Direct Submission.

[1]M.d.W. and G.M.G. contributed equally to this work.

[2]Present address: Research and Innovation, Natural Environment Research Council, SN2 1EU Swindon, United Kingdom.

[3]Present address: Schweizerische Studienstiftung, CH-8032 Zurich, Switzerland.

[4]To whom correspondence should be addressed. Email: christian.fankhauser@unil.ch.

This article contains supporting information online at www.pnas.org/lookup/suppl/doi:10.1073/pnas.1806084115/-/DCSupplemental.

Published online October 1, 2018.

of recovered radiolabeled carbon was similar in plants from both light treatments, a larger fraction of the total amount of assimilated ^{14}C was partitioned toward the elongating internodes of shade-avoiding plants. While this leaf-targeted labeling suggests increased transport from leaves to stem in shade-avoiding plants, C uptake is not controlled in this method and the $^{14}CO_2$ that is released from urea application is also available for fixation in other organs (17).

Steady-state measurements of soluble sugars and starch have produced varied results. Activity of sucrose phosphate synthase, a sucrose biosynthesis enzyme, was increased in leaves of low-R:FR–treated plants (18, 19). Low-R:FR and EOD-FR treatments were shown to increase the amounts of reducing sugars (i.e., glucose and fructose, products of sucrose hydrolysis) in leaves, internodes, and petioles of tobacco (*Nicotiana tabacum*), watermelon (*Citrullus lanatus*), mustard (*Sinapis alba*), and sunflower (*Helianthus annuus*) (15, 16, 20, 21). However, no changes in sucrose levels were found in leaves and petioles of radish plants (*Raphanus sativus*) after long-term low-R:FR treatment (18). Interpretation of steady-state measurements of soluble sugars are complicated by the fact that increased production could increase their concentration, while increased demand in the form of growth would have the opposite effect. Carbohydrates can also be stored in insoluble starch. In leaves, starch is accumulated during the day and degraded at night to provide soluble sugars for metabolism (22). The role of starch in stems is less well defined. Similarly to soluble sugars, the effect of low R/FR on starch accumulation is also apparently variable. Starch granules were found to be smaller and less abundant in chloroplasts of EOD-FR–treated tobacco leaves (*Nicotiana tabacum*) (20) and decreased starch levels were reported in radish (18) after phytochrome inactivation; however, starch was reported to be increased in mustard (16). In accordance with the latter, the constitutive shade-avoiding *phyA phyB phyD phyE Arabidopsis* mutant accumulates more starch per shoot fresh weight during the day, which correlates with reduced daytime shoot growth (23). In contrast, the *phyA phyB* mutant, which showed photosynthesis and fresh weight similar to the wild-type L*er*, was found to accumulate less starch toward the end of the day (24). Interestingly, transcriptomic analyses of the shade avoidance response indicate down-regulation of genes involved in starch metabolism (11, 25).

Photosynthesis-related genes are also down-regulated by the perception of shade signals (25–27). Chlorophyll content per unit leaf area was reduced in EOD-FR–treated tobacco leaves, with chloroplasts containing smaller but more grana (20, 28). Nevertheless, leaf photosynthesis was unaffected by low R:FR and EOD-FR, as net CO_2 uptake and total leaf carbohydrates were similar in control and treated plants (18, 28, 29). In contrast, photosynthetic capacity of tomato stems (*Solanum lycopersicum*), which was about one-third of leaf photosynthetic capacity, was rapidly reduced to almost zero in low R:FR (29). This corresponded to reduced dark respiration and chlorophyll content of the stem (29), suggesting that the photosynthetic apparatus is repressed upon low R:FR perception in this organ. These reports all point toward major metabolic adjustments accompanying elongation growth in low R:FR, although the inconsistencies between studies leave major questions unanswered.

The shade avoidance signaling pathway is extensively studied in plant seedlings. Here, we investigated carbon partitioning during shade avoidance in *Arabidopsis thaliana* and *Brassica rapa* seedlings, analyzing allocation both between organs and between carbon pools within organs. We provide insight into how resources are reallocated to adapt growth patterns to shade conditions.

Results

Low-R:FR Treatment Increases Carbon Allocation from Cotyledons to Hypocotyl. Although *Arabidopsis* hypocotyls may assimilate some carbon locally, the substantial growth that takes place in low-R:FR–treated hypocotyls is expected to require resources from the cotyledons. This, in turn, is likely to impact on cotyledon growth, which is reduced in low R:FR (*SI Appendix*, Fig. S1 *A* and *B*). Using a previously published RNA-seq dataset from 5-d-old *Arabidopsis* seedlings (12), we looked for gene expression patterns related to carbon metabolism that might support a change in resource allocation in low R:FR. After 3 h of low R:FR, expression of several carbon metabolic pathways (photosynthesis, Calvin cycle, sucrose biosynthesis, starch biosynthesis and degradation) was significantly down-regulated in the hypocotyl but remained at a similar level in cotyledons (*SI Appendix*, Fig. S1*C*; see Dataset S1 for gene lists). This organ-specific expression pattern suggests that carbon assimilation and storage might be reduced locally in the hypocotyl in response to low R:FR. The elongating hypocotyl may thus increase in sink strength not only because of its rapid growth but also because of reduced production of local photosynthate.

To study resource allocation during the shade avoidance response directly, we performed radioisotope-labeling experiments to quantitatively study carbon allocation into different organs. The small size of *Arabidopsis* seedlings being an impediment; we used *Brassica rapa* seedlings, which show a shade avoidance response similar to *Arabidopsis* (30, 31). This includes increased hypocotyl elongation and reduced cotyledon expansion (*SI Appendix*, Fig. S2 *A* and *B*), reflected in altered biomass accumulation in both organs (*SI Appendix*, Fig. S2*C*). Accelerated

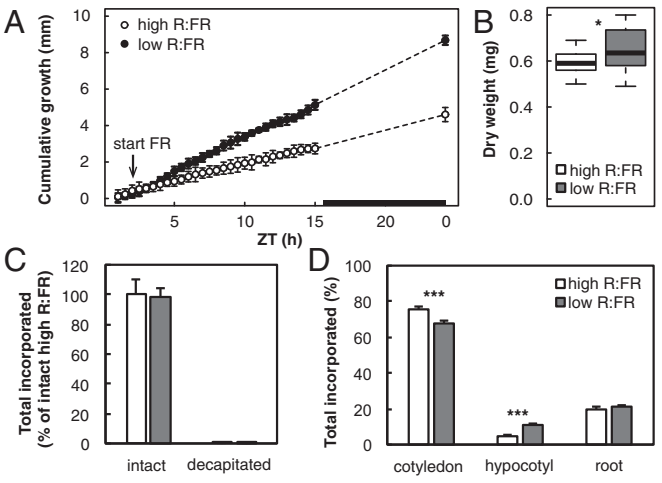

Fig. 1. Resource partitioning between *Brassica rapa* seedling organs after 9 h of light treatment. Five-day-old *B. rapa* seedlings grown in long days were subjected to high or low R:FR at ZT2. (*A*) Hypocotyl growth was measured from time-lapse images with 30-min intervals. The black bar in the *x* axis represents the dark period. Data represent means ± 2 SE; $n = 9$. (*B*) Hypocotyl biomass after 9 h of light treatment. Data are represented as standard boxplots representing median and interquartile (IQR) range between the 25th and 75th percentiles. Whiskers extend to 1.5-fold the IQR; $n = 20$. (*C*) Incorporation of radiolabeled C in intact seedlings or seedlings from which cotyledons had been removed (decapitated), harvested immediately after a 10-min pulse of $^{14}CO_2$ following 9 h of light treatment. Values are expressed as the percentage of label recovered in each sample compared with the average total label of high-R:FR–treated intact plants. Data represent means ± 2 SE; $n = 4$. (*D*) ^{14}C incorporation in cotyledon, hypocotyl, and root tissue after a 1-h chase. Values are expressed as a percentage of total label recovered in each organ. Data represent means ± 2 SE; $n = 4$. Asterisks indicate significant difference. Significance codes: *$0.05 > P > 0.01$, **$0.01 > P > 0.001$, ***$P < 0.001$.

hypocotyl growth was observed after ~2 h of low-R:FR treatment (Fig. 1*A*), similar to what was previously reported in *Arabidopsis* (12, 32). We treated *Brassica* seedlings with a 10-min $^{14}CO_2$ pulse after 9 h of low-R:FR treatment, when clear differences in hypocotyl length and a small but significant increase in hypocotyl dry weight could be detected (Fig. 1*B*). Using such an early time point allowed to focus on early events and minimizes the impact of increased size of the organ on C partitioning.

Total assimilation of CO_2 in low-R:FR–treated plants was unchanged compared with high-R:FR–treated plants (Fig. 1*C*), which indicates that the total amount of carbon available was similar for seedlings in both high and low R:FR. This allowed us to compare carbon fractions of the different light treatments as a percentage of the total amount of label found in a sample. Some carbon was expected to be fixed locally by the hypocotyl, which may influence the calculated partitioning between organs. To calculate this fraction, we provided a $^{14}CO_2$ pulse to seedlings from which the cotyledons were removed immediately before labeling. These "decapitated" hypocotyls were harvested immediately to prevent loss of label through respiration. Compared with intact seedlings, less than 0.5% of the total ^{14}C was assimilated in decapitated hypocotyls (Fig. 1*C*), showing that the vast majority of CO_2 taken up by the plant is assimilated in the cotyledons. After a 1-h chase, more than 75% of the total assimilated ^{14}C was retained in the cotyledons in high R:FR (Fig. 1*D*). Of the 25% allocated to the other organs, 5% was taken up by the hypocotyl and 20% by the roots. Compared with high R:FR, 7% less ^{14}C was found in the cotyledons of low-R:FR–treated seedlings, while ^{14}C in the hypocotyl was increased by the same amount (Fig. 1*D*). As this increase in hypocotyl ^{14}C is much larger than the contribution of local assimilation (Fig. 1*C*), and because total ^{14}C allocated to the roots was unaffected, we conclude that increased ^{14}C in the hypocotyl of low-R:FR–treated seedlings is the direct result of carbon reallocation from the cotyledon.

Carbon Partitioning Within Organs Corresponds With Their Growth Response to Low R:FR. The cotyledon, hypocotyl, and root samples were further fractionated to determine partitioning into different pools of carbon within each organ. Initial fractionation separated into ethanol-soluble, water-soluble, or insoluble components. These three primary fractions in the cotyledons, hypocotyl, and root together contained the entire assimilated label, from which each fraction was calculated as a percentage (Fig. 2). The ethanol-soluble fraction contains predominantly lipids and waxes. The water-soluble fraction was further separated into an acidic fraction (containing mostly phosphorylated sugars and organic acids), a basic fraction (mostly amino acids), and neutral components (mostly neutral sugars). From the insoluble fraction, starch was measured and the remaining label represents assimilated carbon in cell walls and proteins (Fig. 2*D*).

In cotyledons of low-R:FR–treated seedlings, a lower percentage of ^{14}C was committed to starch as well as to protein and cell walls (Fig. 2*A*), which corresponds to the reduced growth of this organ in low R:FR (*SI Appendix*, Fig. S2*B*). There were trends toward less ^{14}C recovery in the rapidly turned-over pool of soluble sugars ($P = 0.050$) and more partitioning into the acidic fraction ($P = 0.060$). These changes are likely due to an increased flux toward sucrose, via sugar phosphates, and faster export of sucrose toward sink organs. In the root, small changes in partitioning were observed, suggesting slightly more commitment to growth after 9 h of low R:FR (Fig. 2*C*).

Strikingly, in low-R:FR–treated plants, increased partitioning to the hypocotyl (Fig. 1*C*) was reflected in all of the downstream carbon pools of this organ (Fig. 2*B*). Only a small proportion of ^{14}C was partitioned into starch; however, this was increased more than fourfold from 0.13 to 0.6% in low R:FR. The neutral fraction increased more than twofold, which is an expected result

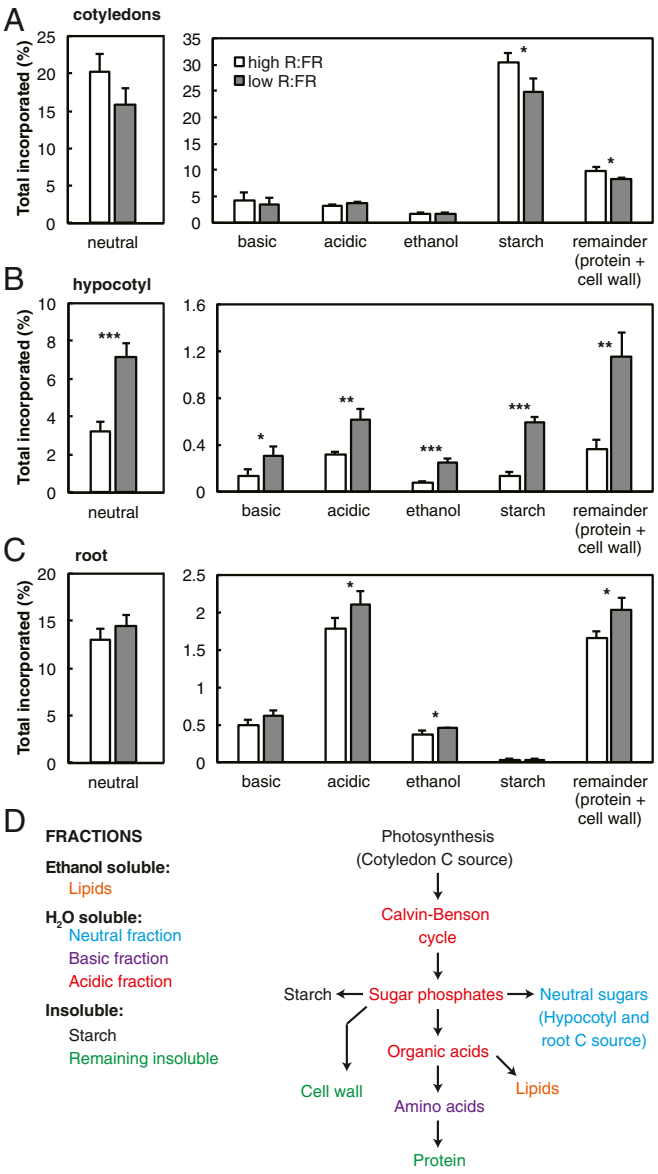

Fig. 2. Carbon partitioning within organs after 9 h of low R:FR. Cotyledon (*A*), hypocotyl (*B*), and root (*C*) samples of 5-d-old seedlings grown in long days, harvested after a 1-h chase following exposure to a 10-min pulse of $^{14}CO_2$, 9 h after start of light treatment. Samples were processed into primary fractions of ethanol-soluble, H_2O-soluble, and insoluble components. The water-soluble fraction was further fractionated into basic, acidic, and neutral fractions and the insoluble fraction into starch and a remaining fraction containing proteins and cell walls (*D*). Data represent means ± 2 SE; $n = 4$. Asterisks indicate significant difference. Significance codes: *$0.05 > P >$ 0.01, **$0.01 > P > 0.001$, and ***$P < 0.001$.

of increased sucrose transport from the cotyledons. The increased allocation to the ethanol-soluble fraction (lipids and cell membranes) and the protein and cell wall-insoluble fraction indicates an increased investment into growth components, corresponding with low-R:FR–induced hypocotyl elongation and biomass accumulation (Fig. 1*C* and *SI Appendix*, Fig. S2 *A* and *C*).

Metabolite Levels Are Stable During the First 24 h of Low-R:FR Treatment. To test whether the observed changes in ^{14}C allocation lead to changes in metabolite levels, we determined sugar concentrations in hypocotyls and cotyledons during the first 24 h

of neighbor detection. Overall, low-R:FR treatment induced little to no significant changes in metabolite levels in both organs (Fig. 3 and *SI Appendix*, Fig. S3). As ^{14}C partitioning increased more than threefold in the ethanol-soluble and -insoluble hypocotyl fractions (Fig. 2 *A* and *B*), it is likely that transported sugars are rapidly utilized to produce the components of growth, cell membranes, cell walls, and proteins and hence do not accumulate. Starch levels in cotyledons showed a typical accumulation during the day and depletion during the night (*SI Appendix*, Fig. S3). Interestingly, the increased partitioning toward starch in the hypocotyl did not result in measurably more starch accumulation (Fig. 3*D*). This may be due to simultaneous starch degradation (i.e., turnover), but we were unable to verify this as maltose, a key intermediate of starch degradation, was below the limit of detection in our analysis. Taken together, increased ^{14}C partitioning toward hypocotyls combined with relatively stable metabolite levels suggests that low R:FR leads to a rapid turnover of metabolites and an increased flux through the measured carbon pools to the end products of growth.

Shade-Induced Hypocotyl Elongation Requires Sucrose Transport. Our partitioning data strongly suggest an increased flow of sucrose from the cotyledons to the hypocotyl in low-R:FR–treated seedlings (Figs. 1*D* and 2). To test whether phloem transport plays a role in the hypocotyl elongation response to low R:FR, we measured hypocotyl lengths of two *Arabidopsis* sucrose transporter mutants. Despite their deficiency in apoplastic phloem loading, 5-d-old *suc2* and *sweet11 sweet12* seedlings showed hypocotyl growth comparable to that of the wild-type Columbia-0 (Col-0) in high R:FR (Fig. 4 *A* and *B*). At this early developmental stage, carbon is derived from seed-lipid catabolism and gluconeogenesis rather than from photosynthesis (33). After these initial 5 d of growth, the *suc2* mutant showed somewhat reduced hypocotyl growth after 3 additional days of high R:FR (Fig. 4*A*), while the *sweet11 sweet12* mutant had a wild-type phenotype. Both mutants had an impaired elongation response compared with the wild type after 3 d of low R:FR with a particularly strong defect in *suc2* (Fig. 4 *A* and *B*). This impaired response was apparent from the start of the treatment. While Col-0 showed a steady increase in absolute hypocotyl growth ~2 h after the start of low-R:FR treatment, this was delayed and much reduced in *suc2*, similar to *sav3*, a mutant that is defective in auxin production (Fig. 4*C*) (34). Adding 1% sucrose to the medium after 5 d of growth increased hypocotyl

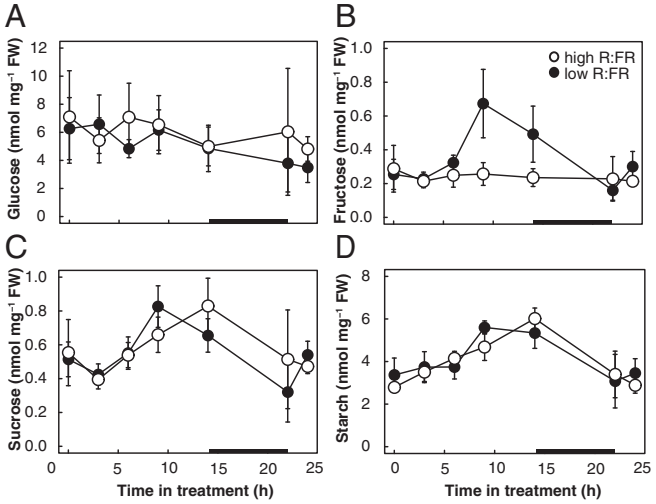

Fig. 3. Metabolite levels in *Brassica rapa* hypocotyls during the first 24 h of the shade avoidance response. Five-day-old *B. rapa* seedlings were grown in long days and subjected to high or low R:FR at ZT2 ($t = 0$). Hypocotyls were analyzed for glucose (*A*), fructose (*B*), sucrose (*C*), and starch (*D*) levels at the indicated time points after the start of low R:FR, including just before dark and immediately after dawn. The black bar in the *x* axis represents the dark period. Data represent means ± 2 SE; $n = 4$ replicates of four pooled seedlings. Corresponding cotyledon data are shown in *SI Appendix*, Fig. S3.

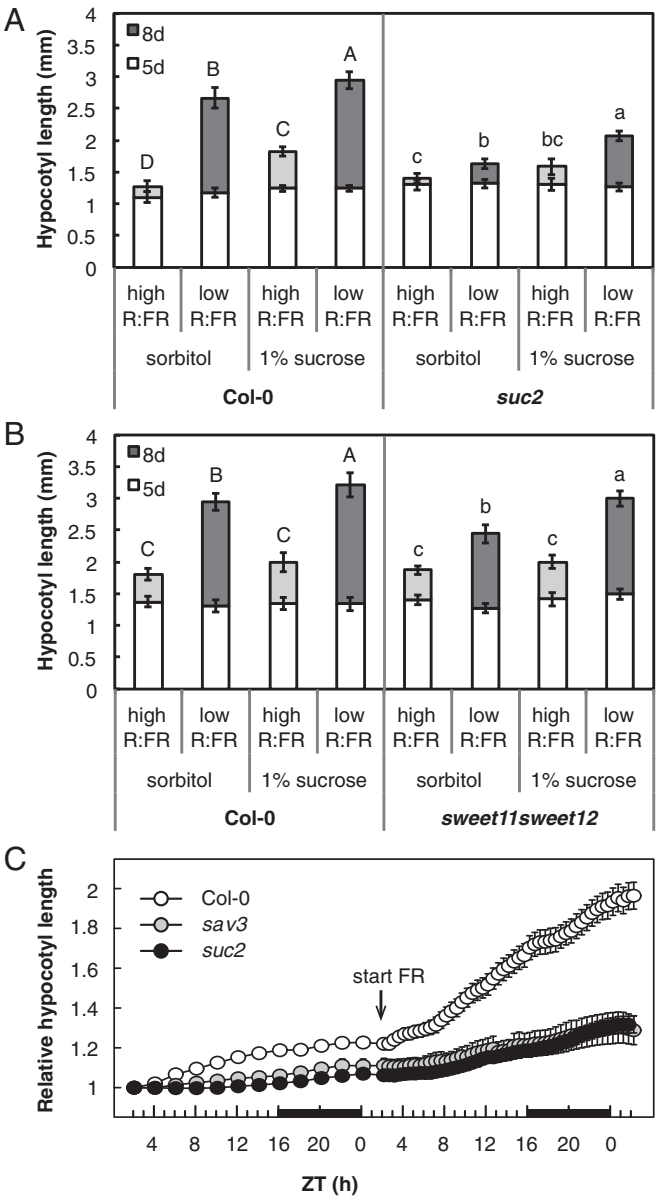

Fig. 4. Shade-induced hypocotyl growth requires sugar transport. Hypocotyl length of sucrose transport mutants *suc2* (*A*) and *sweet11 sweet12* (*B*), grown in long days. Length was measured after 5 d of growth in high R:FR and a subsequent 3 d in high (light gray) or low R:FR (dark gray). Seedlings were transferred to medium supplemented with 1% sucrose or the molar equivalent in sorbitol after 5 d. Data represent means ± 2 SE; $n > 20$. Different letters indicate significant difference after 8 d. Statistics (two-way ANOVA, $P < 0.05$) were split per genotype due to significant interaction effects. (*C*) High-resolution growth analysis of Col-0, *suc2*, and *sav3* seedlings around the start of low-R:FR treatment. Hypocotyl length from long-day grown seedlings was measured from time-lapse images with 2-h intervals starting from ZT2 after 4 d of growth. The next day, images were taken at 30-min intervals after the start of low-R:FR treatment at ZT2. Relative hypocotyl length was calculated by dividing hypocotyl length at each time point by its length at the start of measurements. The black bar in the *x* axis represents the dark period. Data represent means ± 2 SE; $n > 30$.

length in Col-0 particularly in low R:FR and (partially) rescued the low-R:FR hypocotyl response of the sucrose transport mutants (Fig. 4 *A* and *B*). These results suggest that the sucrose transport mutants have a shortage of carbon supply to fuel-enhanced hypocotyl growth after the first 5 d of growth, and confirm that low-R:FR–induced hypocotyl elongation indeed requires rapid source to sink transport of photoassimilates through the phloem.

To test whether perturbed sugar metabolism affects seedling growth, we measured hypocotyl lengths of the *pgi1*, *pgm1*, and *adg2 Arabidopsis* mutants, which are deficient in three subsequent steps of starch biosynthesis, impairing the pathway to varying degrees (*SI Appendix*, Fig. S4). Of these mutants, *pgm1* is known to have increased daytime sucrose levels and increased shoot to root transport in adult plants (35, 36). Starch levels in cotyledons of 8-d-old *pgm1* seedlings were reduced to almost zero, while soluble sugars were increased more than twofold (*SI Appendix*, Fig. S4). *pgi1* cotyledons had intermediate sugar concentrations, with strongly reduced (64%) starch levels and slightly increased soluble sugar content (*SI Appendix*, Fig. S4). Starch levels in *adg2* cotyledons were reduced by only 24%, which may be explained by partial compensation of the structural role conferred by ADG2 by another large subunit (likely APL3) in leaves (37, 38). Soluble sugar levels in *adg2* cotyledons were comparable to those of the wild-type Col-0 (*SI Appendix*, Fig. S4). Interestingly, the sugar concentrations in these mutants did not correspond to their hypocotyl phenotypes. *pgm1* (low-starch, high-soluble sugars) and *adg2* (moderately reduced starch, wild-type soluble sugar levels) had longer hypocotyls than Col-0 in both high and low R:FR, while *pgi1* (reduced starch, increased soluble sugars) had a wild-type phenotype in high R:FR but an impaired low-R:FR response (Fig. 5*A*). These results indicate that hypocotyl growth is indeed affected by perturbed starch biosynthesis, but that this cannot be directly linked to altered total sugar levels in the cotyledons.

Alternatively, the difference between the elongated mutants (*pgm1* and *adg2*) versus the shorter wild type and *pgi1* may be related to the capacity to store starch in the hypocotyl. In heterotrophic tissues such as the hypocotyl, the early step in starch biosynthesis catalyzed by phosphoglucose isomerase (PGI) can be bypassed through the import of glucose 6-phosphate into the plastid, allowing the production of starch in such tissues of the *pgi1* mutant (39). Indeed, the *pgm1* and *adg2* seedlings overall showed no and little starch with iodine staining, respectively, while *pgi1* seedlings accumulated starch in the hypocotyl similarly to the wild type (Fig. 5 *B*–*E*). Consequently, the hypocotyl phenotypes of the starch mutants appear to correspond with their capacity to produce starch in the hypocotyl irrespective of starch and sugar levels in the cotyledons. Failure to partition carbon into hypocotyl starch may thus lead to elongated hypocotyls even in unshaded conditions, as in *pgm1* and *adg2.* This correlation was extended by the analysis of *adg1*, which like *pgm1* has low starch in all tissues. *adg1* seedlings showed no starch accumulation in hypocotyls and had elongated hypocotyls in high R:FR (*SI Appendix*, Fig. S4). All starch mutants, however, maintained a hypocotyl elongation response to low R:FR, likely fueled by resources from the cotyledons. Failure to mobilize starch in the hypocotyl may also inhibit its growth. We therefore tested the starch degradation mutant *sex1*, which is prevented from completely degrading starch during the night in both the leaves and in the hypocotyl (40). Indeed, *sex1* hypocotyls were shorter than wild type in high R:FR and had a reduced response to low R:FR (Fig. 5*F*; two-way ANOVA genotype by light treatment interaction, $P = 0.00015$), which correlated with high starch accumulation in the morning (Fig. 5 *G* and *H*).

PIF7 Is Required for Sucrose-Induced Hypocotyl Elongation. The elongated hypocotyls of *pgm1*, *adg1*, and *adg2* suggest that sugars in the hypocotyl are directed to growth processes if they are not partitioned into the local starch pool. As PIFs have been identified as central integrators of growth (41), we asked whether the PIFs that are required for shade avoidance are involved in this process. Hypocotyl elongation induced by exogenously applied sucrose was previously shown to be impaired in the *pif1 pif3 pif4 pif5* mutant (42–44), and we now investigated the role of PIF7, a central signaling component of the shade avoidance response (9). Sucrose added to the medium did not induce hypocotyl elongation in the *pif7* mutant in high R:FR (Fig. 5*I*), suggesting that PIF7 is indeed important for the regulation of hypocotyl elongation in response to sugar. There was a small elongation response to added sucrose in low R:FR (Fig. 5*I*), which may be due to the action of PIF4 and PIF5 that also promote shade-induced growth (8). Indeed, sucrose responsiveness was abolished in the *pif4 pif5 pif7* mutant, both in high and low R:FR (Fig. 5*I*). A role for PIF7 in the conversion of hypocotyl sugars to growth was further confirmed in the *pgm1 pif7* double mutant. Sugar levels in *pgm1 pif7* were comparable to *pgm1*, with increased soluble sugar concentrations and very low starch levels in both cotyledons and hypocotyl (*SI Appendix*, Fig. S5). Strikingly, while *pgm1* was epistatic over *pif7* with respect to sugar concentrations, *pif7* was epistatic over *pgm1* with respect to hypocotyl growth. Similar to *pif7*, *pgm1 pif7* showed very little growth between days 5 and 8 in high R:FR (Fig. 5*J*). While the double mutant was slightly longer than *pif7* in low R:FR, it was much shorter than *pgm1* in this condition (Fig. 5*J*). Thus, the *pgm1* sugar phenotype is not converted into elongated hypocotyls in a PIF7-deficient background, underlining the importance of PIFs as central regulators of growth in response to both environmental and metabolic signals.

Discussion

The shade avoidance response of elongating stems and reduced leaf growth has often been ascribed to altered resource allocation, but direct evidence for this hypothesis is limited. In previous reports, more radiolabeled carbon from ^{14}C-urea applied to leaves was found to accumulate in internodes of shade-treated plants than in control plants (15, 16). In our experiments, ^{14}C was taken up as $^{14}CO_2$ during photosynthesis, allowing for a defined duration of pulse and chase to study both carbon fixation and its subsequent allocation. Since total ^{14}C assimilation was not affected in low-R:FR–treated *B. rapa* seedlings and hypocotyl photosynthesis contributed only marginally to ^{14}C uptake (Fig. 1*C*), our experiments demonstrate specific resource reallocation from cotyledons to the hypocotyl in shade-avoiding seedlings. Our data indicate that increased allocation to the hypocotyl takes place in the form of sucrose channeled through the phloem (Figs. 2 and 4 *A* and *B*). Consistent with this hypothesis, the *Arabidopsis* mutants in apoplastic phloem loading *suc2* and *sweet11 sweet12* indicate that a downward flux of sucrose is required for low-R:FR–induced hypocotyl elongation (Fig. 4). Interestingly, reduced expression of the sucrose transporter SUT4 in potato *StSUT4-RNAi* plants was previously shown to compromise internode elongation in response to shade, highlighting the importance of this mechanism in several plant species (45). Our kinetic analysis of low-R:FR–induced growth indicates that, similar to indole-3-acetic acid production, sucrose transport is required for rapid shade-induced hypocotyl elongation (Fig. 4*C*) (34).

Overall, the partitioning changes in carbon pools within organs correspond well with their growth response in low R:FR. The increased partitioning toward the hypocotyl in low R:FR did not lead to accumulation of sugars (Fig. 3), which indicates that the flux through the different carbon pools is higher in low R:FR. The increased amount of carbon that reaches the hypocotyl thus appears to be efficiently turned over into growth products, correlating with a hypocotyl-specific increase in gene expression

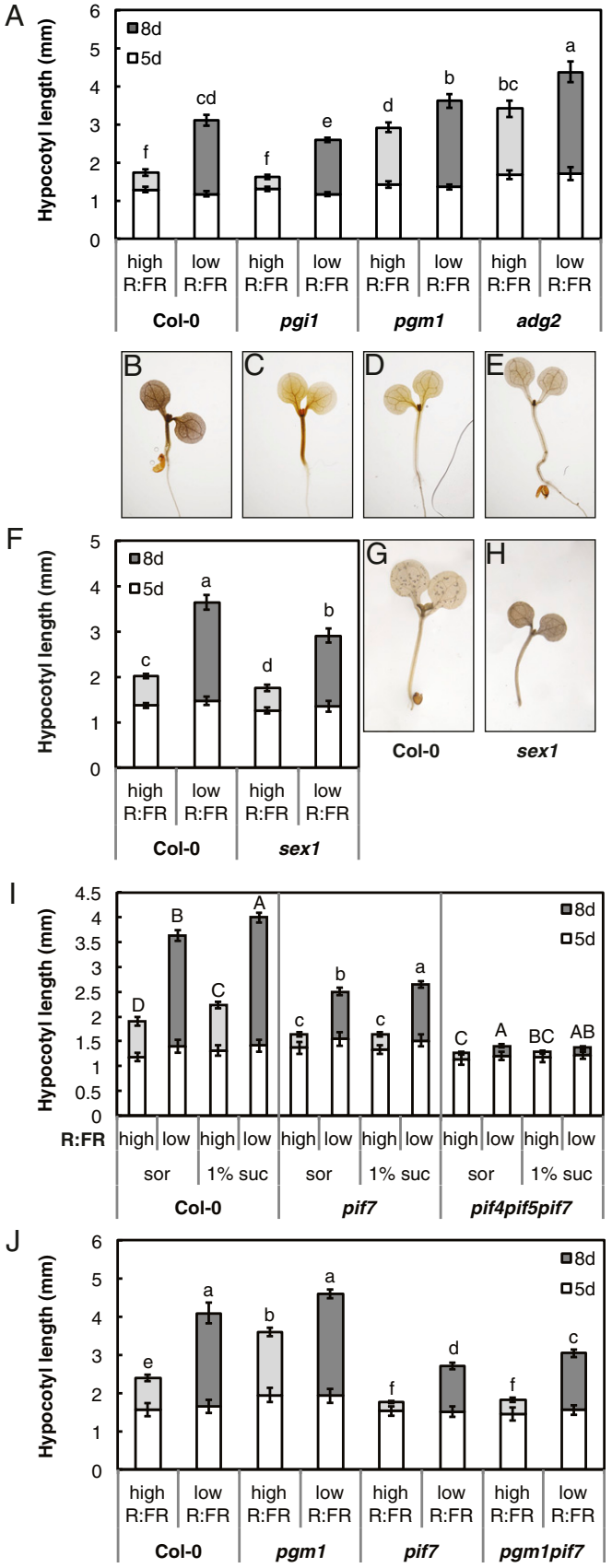

Fig. 5. Shade-regulated hypocotyl growth control involves starch metabolism and PIF7. Hypocotyl length of starch (*A* and *F*) and shade avoidance mutants (*I* and *J*) grown in long days after 5 d of growth in high R:FR and a subsequent 3 d in high (light gray) or low (dark gray) R:FR. Seedlings in *I* were transferred to medium supplemented with 1% sucrose or the molar equivalent in sorbitol after 5 d. Data represent means ± 2 SE; $n > 20$. Different letters indicate significant difference after 8 d. Statistics in *I* (two-way ANOVA, $P < 0.05$) were split per genotype due to significant interaction effects. (*B*–*E*) Iodine staining of starch biosynthesis mutants. Representative picture of Col-0 (*B*), *pgi1* (*C*), *pgm1* (*D*), and *adg2* (*E*) seedlings after 7 d in high R:FR harvested at ZT12. (*G* and *H*) Representative picture at ZT2 of iodine-stained Col-0 (*G*) and *sex1* (*H*) seedlings after 5 d of growth in high R:FR and 2 subsequent days in low R:FR.

related to protein, cell wall, and lipid biosynthesis found previously in low-R:FR–treated *Arabidopsis* seedlings (12).

Increasing sugar levels in the medium leads to modest hypocotyl elongation in the wild type (Figs. 4 *A* and *B* and 5 *I* and *J*). However, the characterization of starch synthesis and degradation mutants suggests that the capacity to store carbon as starch in the hypocotyl may play a role in the conversion of a metabolic signal into growth (Fig. 5). Carbon allocation to hypocotyl starch is increased in low-R:FR–treated seedlings (Fig. 2*A*). This starch is predominantly produced from carbon supplied by the cotyledons as the percentage of ^{14}C partitioned to hypocotyl starch in low R:FR exceeds the amount contributed by hypocotyl photosynthesis (Figs. 1*C* and 2*B*). Furthermore, starch in the *pgi1* mutant cannot be produced from local photosynthate as this reaction links the Calvin cycle to starch production in the chloroplast. Therefore, accumulation of hypocotyl starch in this mutant confirms local starch production from imported carbon (Fig. 4). While partitioning to starch increased in low R:FR, starch levels remained largely unchanged (Fig. 3 and *SI Appendix*, Fig. S3). The unaffected starch accumulation in low-R:FR–treated hypocotyls may indicate that starch is being degraded in the light, a phenomenon recently shown to occur at dusk in *Arabidopsis* leaves (46). While the function of starch as carbon supply for growth and metabolism during the night is well known in leaves, its role in the hypocotyl is not well understood. The diel pattern of starch turnover in *B. rapa* cotyledons was similar to that described for *Arabidopsis* (22) (*SI Appendix*, Fig. S3). Starch turnover in the hypocotyl appeared to be much lower than in the cotyledon. Moreover, a significant proportion was retained at the end of the night, which suggests that the storage of carbohydrates into starch is not vital for the support of hypocotyl growth and metabolism at night (Fig. 3). This is supported by the elongated hypocotyl phenotype of the *Arabidopsis adg1*, *adg2*, and *pgm1* mutants, which display more hypocotyl growth despite accumulating little to no starch in this organ (Fig. 5 and *SI Appendix*, Fig. S4). On the other hand, *pgi1*, a starch biosynthesis mutant accumulating starch in the hypocotyl, does not have an elongated hypocotyl (Fig. 4 *C* and *E*). Finally, in *sex1*, a starch excess mutant with impaired starch degradation, hypocotyl elongation is reduced particularly in low R:FR (Fig. 5*F*). Together, these results suggest that carbon partitioning into hypocotyl starch may act as a growth-buffering mechanism for fluctuating carbon supply from the cotyledons rather than as a major carbohydrate store.

Hypocotyl elongation depends on PIF7, whether it is induced by low R:FR, by exogenous sucrose or by endogenous metabolic signals (Fig. 5 *I* and *J*). PIF7 is known to be an important regulator of shade-induced growth, where it is required for increased auxin levels and responsiveness leading to hypocotyl and petiole elongation (9, 12, 31, 47). Interestingly, sucrose addition to the medium induces a response similar to low R:FR, with increased auxin biosynthesis and enhanced auxin sensitivity (43, 44). The impaired sucrose response in *pif7* hypocotyls may thus result from a deficient auxin response. Furthermore, sucrose may directly promote PIF action through enhanced protein levels and increased promoter binding (43, 48). Hence, PIF7 may also

regulate sugar delivery to the hypocotyl or act locally in the hypocotyl to enable growth enhancement triggered by an increase in sugar availability. While the exact mechanisms orchestrating the channeling of assimilated carbon into hypocotyl growth remain to be identified, it is clear that PIF7 plays a central role in shade and sugar metabolism-regulated growth (Fig. 4 *H* and *I*).

In conclusion, we show substantial resource reallocation and metabolic changes during the shade avoidance response. Our results suggest a model in which low-R:FR–induced hypocotyl elongation requires sucrose transported from the cotyledon and is controlled by regulation (PIF7) and local metabolic buffering (starch). Coordination of carbon partitioning, flux, and metabolite homeostasis appears to be a mechanism to precisely control growth in a situation in which carbon fixation is likely to become limited.

Materials and Methods

Plant Material and Growth Measurements. All *Arabidopsis* plants were in the Col-0 background. We used the following mutants: *pif4 pif5 pif7* (47), *suc2-4* (49), *sweet11 sweet12* (50), *pgi1-1* (39), *adg1-1* (51), *adg2-1* (37), *pgm1-1* (52), *sex1-3* (53), and *sav3-2* (34). The *pgm1 pif7* double mutant was obtained by crossing *pgm1-1* with *pif7-1*. *Arabidopsis* seeds were surface sterilized and placed on top of a nylon mesh on 1/2 Murashige and Skoog (MS) medium (pH 5.7) containing 1.6% (m/vol) agar in square plates. After 3 d of stratification, the square plates were put upright in a Percival incubator at 20 °C in long days with a 16-h light period at 130 $\mu mol \cdot m^{-2} \cdot s^{-1}$ and a R:FR of 1.2 (measured with OceanOptics USB2000+ spectrometer). After 5 d of growth, plates were either kept in this condition, or transferred at Zeitgeber time 2 (ZT2) to a cabinet supplemented with FR LEDs to reach R:FR 0.2 with otherwise identical conditions. For sucrose treatments, the mesh containing the 5-d-old seedlings was transferred to a plate with fresh medium supplemented with 1% sucrose or the molar equivalent in sorbitol as an osmotic control. Hypocotyl length was measured from pictures after 5 and 8 d of growth with a customized MATLAB script developed in the C.F. laboratory. Time-lapse imaging was conducted as described in ref. 12, with the following differences: high-R:FR–grown seedlings were imaged at 2-h intervals from the fourth to the fifth day of growth. After transfer to low R:FR on ZT2 on the fifth day, images were taken every 30 min. Hypocotyl length was measured using an improved semiautomated MATLAB script. Relative hypocotyl length was calculated as hypocotyl length at each time point divided by hypocotyl length of the same seedling at the beginning of measurements on the fifth day.

For *Brassica rapa* experiments, the strain R-*o*-18 was used. For growth and metabolite measurements, *B. rapa* seeds were surface-sterilized and placed in square plates filled up to 3 cm with 1/2 MS medium containing 1.6% (m/vol) agar (pH 5.7), allowing the seedlings to grow vertically in the space not containing medium. After 2 d of stratification, a similar protocol as for *Arabidopsis* was followed, with plates divided over high and low R:FR after 5 d of initial growth in high R:FR. Hypocotyl length and cotyledon area were measured with customized MATLAB scripts for *B. rapa*. For growth kinetics, nine seedlings per treatment were photographed every 30 min during the light period using the time-lapse setup described in ref. 12. Cumulative growth was calculated as the sum of length increase between time points, averaging three consecutive time points in a sliding window to smooth the data for visualization. For biomass measurements, cotyledons and hypocotyls were dissected and dried separately at 60 °C for at least 48 h.

For labeling experiments, *B. rapa* seedlings were grown in enclosed, transparent plastic containers (Phytatray II; Sigma-Aldrich; length by width by height, 11.4 × 8.6 × 10.2 cm). Eight sterilized seeds per box were lightly pressed into a layer of 100 mL of 1/2 MS 0.8% (m/vol) agar (pH 5.7). The seeds were stratified for 2 d before transfer to a Percival growth cabinet. During germination and growth, the plants were supplied with 16-h photoperiod with 150 $\mu mol \cdot m^{-2} \cdot s^{-1}$ light intensity. After 5 d of growth, plants were split into two isolated compartments in the growth cabinet, one receiving high R:FR and the other supplemented with FR LEDs to reach low R:FR of 0.1. The plants were allowed to grow for a further 9 h or 3 d before labeling.

Metabolic Pathway Enrichment. To test whether low R:FR induced a coherent up- or down-regulation of genes involved in pathways associated with resource partitioning and allocation, we used the organ-specific transcriptomics dataset described in ref. 12. We considered the pathways related to photosynthetic activity and starch metabolism from the Plant Metabolic Network database (AraCyc, version 15.0; ref. 54). For each pathway and condition, we assigned a score to the pathway computed as $-\sum_i \log(p_i)\mathrm{sign}(f_i)$, where p_i is the *P* value of differential expression between the low-R:FR and high-R:FR condition for gene *i* in the pathway and f_i is the corresponding log fold change. From the expressed protein-coding genes, we then randomly selected half a million sets of the same size and computed their score to assess the empirical *P* value associated with the selected pathway. A Bonferroni correction for multiple pathway testing was applied to identify down- and up-regulated pathways.

Analysis of Carbon Partitioning by $^{14}CO_2$ Labeling. Labeling of photosynthetic products in *B. rapa* seedlings was performed using $^{14}CO_2$ as previously described (55), with several modifications. Immediately before the experiment, phytatrays containing the seedlings were opened and transferred to a custom-built, sealed, transparent chamber, lit with fluorescent lighting (150 $\mu mol \cdot m^{-2} \cdot s^{-1}$). $^{14}CO_2$ was released through the addition of lactic acid to $NaH^{14}CO_3$ (Hartmann Analytic). After 10 min, labeling was stopped by opening the chamber in a fume hood to clear the $^{14}CO_2$. Phytatrays were closed again for the 1-h chase before harvest during which time plants were allowed to metabolize the assimilated carbon. Cotyledons, hypocotyls, or roots from three seedlings were pooled per replicate, and weighed before being submerged in 2 mL of preheated 80% (vol/vol) ethanol for 20 min at 80 °C. The samples were homogenized in a all-glass homogenizer and the soluble and insoluble fractions separated by centrifugation [2,400 × *g*, 12 min, room temperature (RT)]. Sequential extractions of the remaining pellet were performed with 1 mL of 50%, 20%, 0%, and then 80% (vol/vol) ethanol. The pellet was suspended in 1 mL of H_2O, yielding the insoluble fraction from which relative partitioning into starch and protein with cell wall could be determined as described by ref. 56. The soluble fractions were pooled concentrated under vacuum. A water-soluble subfraction was collected by dissolving the near-dry exsiccate in 2 mL of ddH_2O collected after centrifugation (2,400 × *g*, 1 min) while the remainder was dissolved in 2 mL of 98% (vol/vol) ethanol, yielding the wax and lipid fraction. Basic, acidic, and neutral fractions were separated from the water-soluble fraction by ion-exchange chromatography as described by ref. 57. Incorporation of $^{14}CO_2$ into each fraction was measured by liquid scintillation counting by a Tricarb 2100 (Toplab).

Iodine Staining. Seedlings were harvested at the end of the light period after 7 d of growth and heated in 80% (vol/vol) ethanol. When cleared of chlorophyll, seedlings were stained in Lugol solution (I_2/KI; Sigma-Aldrich) for 5 min. Samples were subsequently rinsed in tap water for 2 min and immediately mounted under the stereomicroscope (Nikon SMZ1500 with associated Nikon D7000 camera) for imaging.

Sugar Measurements. Soluble sugars were extracted as described in ref. 58 with minor modifications. Aliquots of 50–80 mg fresh weight (FW) were extracted in ice-cold $CHCl_3$/CH_3OH (3:7, vol/vol), in a ratio of 710 μL of $CHCl_3$/CH_3OH (3:7, vol/vol) per 50 mg FW. As an internal standard, $CHCl_3$/CH_3OH (3:7, vol/vol) was spiked with cellobiose (1 nmol of cellobiose/mg plant FW). After warming to −20 °C with vigorous shaking and incubation for 2 h at −20 °C with occasional vortexing, 710 μL of water/50 mg FW was added and samples were warmed to 4 °C with repeated shaking. Separation of the upper aqueous-CH_3OH phase from the lower $CHCl_3$ phase was achieved by centrifugation at 15,000 × *g* for 5 min at 4 °C. The aqueous-CH_3OH phase was collected, evaporated to dryness at 30 °C, and redissolved in 500 μL of water.

To also extract the insoluble components (including starch) contained in the lower $CHCl_3$ phase, the protocol described in ref. 58 was adapted as follows. The $CHCl_3$ phase was washed with 1 mL of 70% ethanol (% vol/vol) by thorough vortexing. After centrifugation at 20,000 × *g* for 5 min at RT, ethanol was removed. The pellet was dried at 20 °C for 15 min and resuspended in 500 μL of water. Starch was digested as described in ref. 59. After the starch digest, samples were spiked with cellobiose (1.0 nmol of cellobiose/mg plant FW) as an internal standard. All samples were passed through sequential ion exchange columns (Dowex), and the eluted soluble sugars were quantified using high-performance anion-exchange chromatography with pulsed amperometric detection as described previously (59). For extraction of sugars from *Arabidopsis* seedlings, five 8-d-old cotyledons were harvested 8 h into the photoperiod and pooled per replicate. Soluble sugars were extracted through the sequential addition of 2 × 250 μL of 80% (vol/vol) ethanol and a final extraction with 50% (vol/vol) ethanol. Each extraction was performed for 30 min at 80 °C with orbital shaking at 600 rpm. The sequential ethanolic extracts were pooled and dried under vacuum. Starch, remaining in the plantlets, was solubilized in 400 μL of 0.2 M KOH at 95 °C for 1 h. Once

cooled to 20 °C, the solution was neutralized with 70 μL of 1 M acetic acid. Starch and soluble sugars were measured spectrophotometrically using enzyme-linked assays as described in refs. 60 and 61.

ACKNOWLEDGMENTS. We thank Gail Taylor for hosting M.d.W. at the University of Southampton during manuscript preparation. G.M.G., B.D.-E., and S.C.Z. gratefully acknowledge Michaela Fischer-Stettler for her contribution to the maintenance and management of the isotope laboratory. We are grateful to Norbert Sauer for kindly providing *suc2-4* seeds, to Wolf Frommer for *sweet11 sweet12* seeds, and to Lars Ostergaard for *B. rapa* seeds. We thank Bjorn Robroek from the Ecological Systems Laboratory at the École Polytechnique Fédérale de Lausanne for help with dry weight measurements and Prashant Saxena (Indian Institute of Technology) and Kutalmis Gokalp Ince (Middle East Technical University) for developing the MATLAB script for hypocotyl length measurements. Research in the C.F. laboratory was funded by the Swiss National Science Foundation (Grants 31003A_160326 and 310030B_179558), SystemsX.ch (PlantMechanix 51RT-0_145716), and the University of Lausanne. G.M.G., B.D.-E., and S.C.Z. gratefully acknowledge funding from ETH Zürich, the Zürich–Basel Plant Science Centre Plant Fellows Programme (Marie Skłodowska-Curie Action Grant GA-2010-267243), and SystemsX.ch (PlantMechanix 51RT-0_145716).

1. Casal JJ (2013) Photoreceptor signaling networks in plant responses to shade. *Annu Rev Plant Biol* 64:403–427.
2. Morelli G, Ruberti I (2002) Light and shade in the photocontrol of *Arabidopsis* growth. *Trends Plant Sci* 7:399–404.
3. Kebrom TH, Brutnell TP (2007) The molecular analysis of the shade avoidance syndrome in the grasses has begun. *J Exp Bot* 58:3079–3089.
4. Franklin KA (2008) Shade avoidance. *New Phytol* 179:930–944.
5. Finlayson SA, Krishnareddy SR, Kebrom TH, Casal JJ (2010) Phytochrome regulation of branching in *Arabidopsis*. *Plant Physiol* 152:1914–1927.
6. Poorter H, et al. (2015) How does biomass distribution change with size and differ among species? An analysis for 1200 plant species from five continents. *New Phytol* 208:736–749.
7. Wang H, Wang H (2015) Phytochrome signaling: Time to tighten up the loose ends. *Mol Plant* 8:540–551.
8. Lorrain S, Allen T, Duek PD, Whitelam GC, Fankhauser C (2008) Phytochrome-mediated inhibition of shade avoidance involves degradation of growth-promoting bHLH transcription factors. *Plant J* 53:312–323.
9. Li L, et al. (2012) Linking photoreceptor excitation to changes in plant architecture. *Genes Dev* 26:785–790.
10. Hornitschek P, et al. (2012) Phytochrome interacting factors 4 and 5 control seedling growth in changing light conditions by directly controlling auxin signaling. *Plant J* 71: 699–711.
11. Sellaro R, Pacín M, Casal JJ (2017) Meta-analysis of the transcriptome reveals a core set of shade-avoidance genes in *Arabidopsis*. *Photochem Photobiol* 93:692–702.
12. Kohnen MV, et al. (2016) Neighbor detection induces organ-specific transcriptomes, revealing patterns underlying hypocotyl-specific growth. *Plant Cell* 28:2889–2904.
13. Ruan YL (2014) Sucrose metabolism: Gateway to diverse carbon use and sugar signaling. *Annu Rev Plant Biol* 65:33–67.
14. Yu SM, Lo SF, Ho TD (2015) Source-sink communication: Regulated by hormone, nutrient, and stress cross-signaling. *Trends Plant Sci* 20:844–857.
15. Mazzella MA, Zanor MI, Fernie AR, Casal JJ (2008) Metabolic responses to red/far-red ratio and ontogeny show poor correlation with the growth rate of sunflower stems. *J Exp Bot* 59:2469–2477.
16. Casal JJ, Sanchez RA, Paganelliblau AR, Izaguirre M (1995) Phytochrome effects on stem carbon gain in light-grown mustard seedlings are not simply the result of stem extension-growth responses. *Physiol Plant* 94:187–196.
17. Clifford PE, Marshall C, Sagar GR (1973) Examination of value of C-14-urea as a source of Co2-14 for studies of assimilate distribution. *Ann Bot (Lond)* 37:37–44.
18. Keiller D, Smith H (1989) Control of carbon partitioning by light quality mediated by phytochrome. *Plant Sci* 63:25–29.
19. Yanovsky MJ, Casal JJ, Salerno GL, Sanchez RA (1995) Are phytochrome-mediated effects on leaf growth, carbon partitioning and extractable sucrose-phosphate synthase activity the mere consequence of stem-growth responses in light-grown mustard. *J Exp Bot* 46:753–757.
20. Kasperbauer MJ, Hamilton JL (1984) Chloroplast structure and starch grain accumulation in leaves that received different red and far-red levels during development. *Plant Physiol* 74:967–970.
21. Ranwala NKD, Decoteau DR, Ranwala AP, Miller WB (2002) Changes in soluble carbohydrates during phytochrome-regulated petiole elongation in watermelon seedlings. *Plant Growth Regul* 38:157–163.
22. Stitt M, Zeeman SC (2012) Starch turnover: Pathways, regulation and role in growth. *Curr Opin Plant Biol* 15:282–292.
23. Yang D, Seaton DD, Krahmer J, Halliday KJ (2016) Photoreceptor effects on plant biomass, resource allocation, and metabolic state. *Proc Natl Acad Sci USA* 113: 7667–7672.
24. Han X, et al. (2017) Phytochrome A and B regulate primary metabolism in *Arabidopsis* leaves in response to light. *Front Plant Sci* 8:1394.
25. Pacín M, Semmoloni M, Legris M, Finlayson SA, Casal JJ (2016) Convergence of constitutive photomorphogenesis 1 and phytochrome interacting factor signalling during shade avoidance. *New Phytol* 211:967–979.
26. Devlin PF, Yanovsky MJ, Kay SA (2003) A genomic analysis of the shade avoidance response in *Arabidopsis*. *Plant Physiol* 133:1617–1629.
27. Das D, St Onge KR, Voesenek LA, Pierik R, Sasidharan R (2016) Ethylene- and shade-induced hypocotyl elongation share transcriptome patterns and functional regulators. *Plant Physiol* 172:718–733.
28. Kasperbauer MJ, Peaslee DE (1973) Morphology and photosynthetic efficiency of tobacco leaves that received end-of-day red and far red light during development. *Plant Physiol* 52:440–442.
29. Cagnola JI, Ploschuk E, Benech-Arnold T, Finlayson SA, Casal JJ (2012) Stem transcriptome reveals mechanisms to reduce the energetic cost of shade-avoidance responses in tomato. *Plant Physiol* 160:1110–1119.
30. Robson P, Whitelam GC, Smith H (1993) Selected components of the shade-avoidance syndrome are displayed in a normal manner in mutants of *Arabidopsis thaliana* and *Brassica rapa* deficient in phytochrome B. *Plant Physiol* 102:1179–1184.
31. Procko C, Crenshaw CM, Ljung K, Noel JP, Chory J (2014) Cotyledon-generated auxin is required for shade-induced hypocotyl growth in *Brassica rapa*. *Plant Physiol* 165: 1285–1301.
32. Cole B, Kay SA, Chory J (2011) Automated analysis of hypocotyl growth dynamics during shade avoidance in *Arabidopsis*. *Plant J* 65:991–1000.
33. Eastmond PJ (2006) SUGAR-DEPENDENT1 encodes a patatin domain triacylglycerol lipase that initiates storage oil breakdown in germinating *Arabidopsis* seeds. *Plant Cell* 18:665–675.
34. Tao Y, et al. (2008) Rapid synthesis of auxin via a new tryptophan-dependent pathway is required for shade avoidance in plants. *Cell* 133:164–176.
35. Brauner K, Hörmiller I, Nägele T, Heyer AG (2014) Exaggerated root respiration accounts for growth retardation in a starchless mutant of *Arabidopsis thaliana*. *Plant J* 79:82–91.
36. Kölling K, Thalmann M, Müller A, Jenny C, Zeeman SC (2015) Carbon partitioning in Arabidopsis thaliana is a dynamic process controlled by the plants metabolic status and its circadian clock. *Plant Cell Environ* 38:1965–1979.
37. Lin TP, Caspar T, Somerville C, Preiss J (1988) Isolation and characterization of a starchless mutant of Arabidopsis thaliana (L.) heynh lacking ADPglucose pyrophosphorylase activity. *Plant Physiol* 86:1131–1135.
38. Fritzius T, Aeschbacher R, Wiemken A, Wingler A (2001) Induction of ApL3 expression by trehalose complements the starch-deficient Arabidopsis mutant adg2-1 lacking ApL1, the large subunit of ADP-glucose pyrophosphorylase. *Plant Physiol* 126: 883–889.
39. Yu TS, Lue WL, Wang SM, Chen J (2000) Mutation of *Arabidopsis* plastid phosphoglucose isomerase affects leaf starch synthesis and floral initiation. *Plant Physiol* 123: 319–326.
40. Vitha S, Yang M, Sack FD, Kiss JZ (2007) Gravitropism in the starch excess mutant of *Arabidopsis thaliana*. *Am J Bot* 94:590–598.
41. Leivar P, Monte E (2014) PIFs: Systems integrators in plant development. *Plant Cell* 26: 56–78.
42. Stewart JL, Maloof JN, Nemhauser JL (2011) PIF genes mediate the effect of sucrose on seedling growth dynamics. *PLoS One* 6:e19894.
43. Lilley JL, Gee CW, Sairanen I, Ljung K, Nemhauser JL (2012) An endogenous carbon-sensing pathway triggers increased auxin flux and hypocotyl elongation. *Plant Physiol* 160:2261–2270.
44. Sairanen I, et al. (2012) Soluble carbohydrates regulate auxin biosynthesis via PIF proteins in *Arabidopsis*. *Plant Cell* 24:4907–4916.
45. Chincinska IA, et al. (2008) Sucrose transporter StSUT4 from potato affects flowering, tuberization, and shade avoidance response. *Plant Physiol* 146:515–528.
46. Fernandez O, et al. (2017) Leaf starch turnover occurs in long days and in falling light at the end of the day. *Plant Physiol* 174:2199–2212.
47. de Wit M, Ljung K, Fankhauser C (2015) Contrasting growth responses in lamina and petiole during neighbor detection depend on differential auxin responsiveness rather than different auxin levels. *New Phytol* 208:198–209.
48. Shor E, Paik I, Kangisser S, Green R, Huq E (2017) Phytochrome interacting factors mediate metabolic control of the circadian system in *Arabidopsis*. *New Phytol* 215: 217–228.
49. Srivastava AC, Ganesan S, Ismail IO, Ayre BG (2008) Functional characterization of the *Arabidopsis* AtSUC2 Sucrose/H+ symporter by tissue-specific complementation reveals an essential role in phloem loading but not in long-distance transport. *Plant Physiol* 148:200–211.
50. Chen LQ, et al. (2012) Sucrose efflux mediated by SWEET proteins as a key step for phloem transport. *Science* 335:207–211.
51. Wang SM, et al. (1998) Characterization of ADG1, an *Arabidopsis* locus encoding for ADPG pyrophosphorylase small subunit, demonstrates that the presence of the small subunit is required for large subunit stability. *Plant J* 13:63–70.
52. Caspar T, Huber SC, Somerville C (1985) Alterations in growth, photosynthesis, and respiration in a starchless mutant of *Arabidopsis thaliana* (L.) deficient in chloroplast phosphoglucomutase activity. *Plant Physiol* 79:11–17.
53. Yu TS, et al. (2001) The *Arabidopsis sex1* mutant is defective in the R1 protein, a general regulator of starch degradation in plants, and not in the chloroplast hexose transporter. *Plant Cell* 13:1907–1918.
54. Mueller LA, Zhang P, Rhee SY (2003) AraCyc: A biochemical pathway database for *Arabidopsis*. *Plant Physiol* 132:453–460.
55. Kölling K, Müller A, Flütsch P, Zeeman SC (2013) A device for single leaf labelling with CO_2 isotopes to study carbon allocation and partitioning in *Arabidopsis thaliana*. *Plant Methods* 9:45.

56. Zeeman SC, Ap Rees T (1999) Changes in carbohydrate metabolism and assimilate export in starch-excess mutants of *Arabidopsis*. *Plant Cell Environ* 22:1445–1453.
57. Quick P, Siegl G, Neuhaus E, Feil R, Stitt M (1989) Short-term water stress leads to a stimulation of sucrose synthesis by activating sucrose-phosphate synthase. *Planta* 177: 535–546.
58. Arrivault S, et al. (2009) Use of reverse-phase liquid chromatography, linked to tandem mass spectrometry, to profile the Calvin cycle and other metabolic intermediates in *Arabidopsis* rosettes at different carbon dioxide concentrations. *Plant J* 59:826–839.
59. Egli B, Kölling K, Köhler C, Zeeman SC, Streb S (2010) Loss of cytosolic phosphoglucomutase compromises gametophyte development in *Arabidopsis*. *Plant Physiol* 154: 1659–1671.
60. Müller-Röber B, Sonnewald U, Willmitzer L (1992) Inhibition of the ADP-glucose pyrophosphorylase in transgenic potatoes leads to sugar-storing tubers and influences tuber formation and expression of tuber storage protein genes. *EMBO J* 11:1229–1238.
61. Hostettler C, et al. (2011) Analysis of starch metabolism in chloroplasts. *Methods Mol Biol* 775:387–410.